Article ID: 1006-8775(2016) 03-0341-11

SENSITIVITY OF LANDFALLING TYPHOON STRUCTURE AND PRECIPITATION TO VARYING CLOUD MICROPHYSICAL PROCESSES

HUA Cong (花 丛), LIU Qi-jun (刘奇俊)
(National Meteorological Center, Beijing 100081 China)

Abstract: Typhoon KROSA in 2007 is simulated using GRAPES, a mesoscale numerical model, in which a two-parameter mixed-phase microphysics scheme is implanted. A series of numerical experiments are designed to test the sensitivity of landfalling typhoon structure and precipitation to varying cloud microphysics and latent heat release. It is found that typhoon track is sensitive to different microphysical processes and latent heat release. The cloud structures of simulated cyclones can be quite different with that of varying microphysical processes. Graupel particles play an important role in the formation of local heavy rainfall and the maintenance of spiral rainbands. Analysis reveals that the feedback of latent heat to dynamic fields can significantly change the content and distribution of cloud hydrometeors, thus having an impact on surface precipitation.

Key words: cloud microphysics; GRAPES model; landfalling typhoon; latent heat
CLC number: P444 **Document code:** A
doi: 10.16555/j.1006-8775.2016.03.008

1 INTRODUCTION

Tropical cyclones (TCs) and the accompanying heavy rainfall are one of the major contributors to disasters in China. Significant progress has been made in research associated with typhoon storms (Dong et al. [1]; Li et al.[2]; Chen et al.[3]). In terms of analyzing the formation and feature of heavy rainfall brought by TCs, past studies focus on dynamic and thermodynamic progresses caused by interactions between large and mesoscale systems. With the continuous development of numerical models and improvement of model resolution, convections in mesoscale models can be described by explicit microphysics progress, thereby increasing the ability to simulate precipitation (Zhang [4]). More and more studies have found that cloud physics plays an important role in the realness of simulation cyclones.

The cloud structures of cyclones are very sensitive to microphysics progress. Wang found that both evaporation of rain and melting of snow and graupel were responsible for the generation of downdrafts and rainbands [5]. Zhu and Zhang reported that turning off the evaporation of cloud water and rainwater leaded to the most rapid deepening storm with smallest radius but a wider eyewall and strongest eyewall updrafts[6]. Cloud physical processes also have some impact on precipitation structure. Franklin et al. suggested that graupel was an important factor in affecting precipitation structure [7]. Increasing the fall speeds saw producing higher rain rates in inner core of storm. A larger region of stratiform precipitation was produced when the efficiency for collection of snow and cloud ice by graupel was reduced and when the mean size of graupel was reduced. Cheng et al. also pointed out that halving the fall speeds of graupel resulted in maximum of precipitation region, as well as the proportion of non-convective precipitation [8]. The above studies generally based on ideal TCs or offshore TCs. During landfalling progress, due to the interaction of continental shelf and coastal topography, the typhoon track, intensity and distribution of wind and rain will change. Thus with the use of a mesoscale model in which several explicit cloud microphysics schemes are implanted, both evolution and distribution of cloud and precipitation and impact of cloud microphysical processes to typhoon strength, structure, and heavy precipitation can be studied.

Super typhoon Krosa (2007) first appeared over the ocean east of Luzon in the Philippines at 0000 Coordinated Universal Time (UTC) 2 October 2007, and at 1800 UTC 4 October Krosa strengthened into a super typhoon. At 0730 UTC 7 October, Krosa made landfall at Xiaguan town located at the junction of Fujian and Zhejiang provinces, with a central pressure of 975 hPa. After that, Krosa weakened into a strong tropical storm and moved northeastward along the Zhejiang coastline. Krosa returned to the East China Sea at 0930 UTC 8 October and damped into a tropical depression at 1500 UTC 8 October. Krosa was strong

Received 2014-04-24; **Revised** 2016-05-06; **Accepted** 2016-07-15
Foundation item: Special Found for Meteorological Research in the Public Interest (GYHY201506008): Study on Parameterization of Boundary Layer Stratocumulus Process of GRAPES Model
Biography: LIU Qi-jun, Ph. D., Researcher, primarily undertaking research on numerical weather prediction and cloud physics
Corresponding author: LIU Qi-jun, e-mail: liuqj@cma.gov.cn

and stayed over the mainland of China for 26 hours, which was rarely seen in the same period of history. Its long-term effects brought heavy rainfall to north Fujian and most of Zhejiang province.

Krosa had been simulated by Hua and Liu using GRAPES, a triply nested mesoscale numerical model in which a two-parameter mixed-phase microphysics scheme was implanted [9]. It was shown that GRAPES reproduced reasonably well the track, precipitation evolution and cloud microphysical features. Based on preliminary work, a series of numerical experiments are designed to test the sensitivity of landfalling typhoon structure and precipitation to varying cloud microphysics and latent heat release in this study.

2 EXPERIMENT DESIGN

Here we use the GRAPES-Meso model with a two-moment mixed-phase microphysics scheme (Hua and Liu[9]; Chen[10]). The T213 forecast field incorporated with a bogus vortex is adopted as initial field. A triply nested, one-way mode is used in the simulation, and the start and end time for Domain 3 are 0600 UTC 7 October and 0600 UTC 8 October respectively with a horizontal resolution of 3.3km. The simulation region covers five provinces in East China, and only an explicit microphysics scheme is used in Domain 3. Four numerical experiments are designed to test the effects of variations in cloud microphysics and latent heat release on the typhoon structure and precipitation (Table 1). The control experiment (CTL) is identical to the experiment discussed in Hua and Liu [9]. In the experiment WMR, only warm-rain processes and accompanying latent heat release are retained in the cloud microphysics parameterization in order to examine to what extent the precipitation are affected by ice particles (Wang[5]; Zhu and Zhang[6]; Franklin et al.[7]; Wang and Yin[11]). As can be seen from previous studies (Mccumber et al.[12]; Hu and He [13]; Yu et al.[14]), in the region where stronger updrafts exist, graupel particles play an important role as main source in the forming of precipitation. Thus removing graupel and its associated melting and sublimation processes from control run (NGP) is to verify the importance of graupel particles. Under certain dynamic and microphysical conditions, hail process is often observed in strong convective precipitation. As the largest ice particles, hail has complex formation process and greater fall speed. Hail particles and its associated microphysical process are added to CTL in experiment HAIL (Hu and He[13]; Yu et al. [14]), including sublimation and evaporation of hail (S_{vh}), collection of hail and cloud droplets (C_{ch}), hail and ice crystals (C_{ih}), hail and snow crystals (C_{sh}), hail and raindrops (C_{rh}), and hail and graupel (C_{gh}), automatic conversion of graupel to hail (A_{gh}), melting of hail to raindrops (M_{hr}), as well as the limitation of dry growth of hail (C_{wh}). Sub script letters denote the quantities consumed and generated. The equation for sources and sinks is given by

$$\frac{\delta Q_h}{\delta t} = S_{vh} + C_{ih} + C_{sh} + C_{gh} - M_{hr} + A_{gh}$$

where $C=C_{ch}+C_{rh}$ when $T<T_0$, $kk=0$ and $C=C_{wh}$ when $T<T_0$, $kk=1$. T_0=273.15 K and kk indicates hail growth status. When the collection of hail and supercooled water droplets exceeds the C_{wh}, the extra part ($C_{ch}+C_{rh}-C_{wh}$) will form a film on the surface of hail, $kk=1$. Otherwise $kk=0$.

Table 1. Summary of the experimental design

Expt.	Description
CTL	Control experiment using two-parameter mixed-phase microphysics scheme
WMR	As in CTL but only the warm-rain processes are included in the cloud microphysics scheme
NGP	As in CTL but without graupel processes
HAIL	As in CTL but with hail processes
NLH	As in CTL but without latent heat release

Latent heat released by phase change is an important energy source for the maintenance of typhoon intensity and spiral rainbands. All the latent heat release is turned off from the CTL in experiment NLH, which means the removal of feedback from microphysics to temperature changes.

3 NUMERICAL RESULTS

3.1 *Intensity and track*

Figure 1 compares the minimum central pressure between observed and simulated storm. Even though the storm intensity of initial field (with bogus vortex) is weaker than observed, model results and observed intensity are much alike during the heavy precipitation period (shown in the dash box). Therefore, the model results are considered applicable. Throughout the simulation, intensity in WMR, NGP and HAIL goes well with that in CTL, while the central pressure in NLH is lower than other experiments. To the end of the simulation, the central pressure in NLH is 10 hPa lower than CTL with a value of 986 hPa.

Ding pointed out that during the formation of TCs, large amount of latent heat is released by the condensation of water vapor [15]. Mid-upper level troposphere can be effectively heated by the latent heat, and as a result the central pressure of tropical disturbance continuously goes lower and the storm grows stronger. Seen from the vertical distribution of

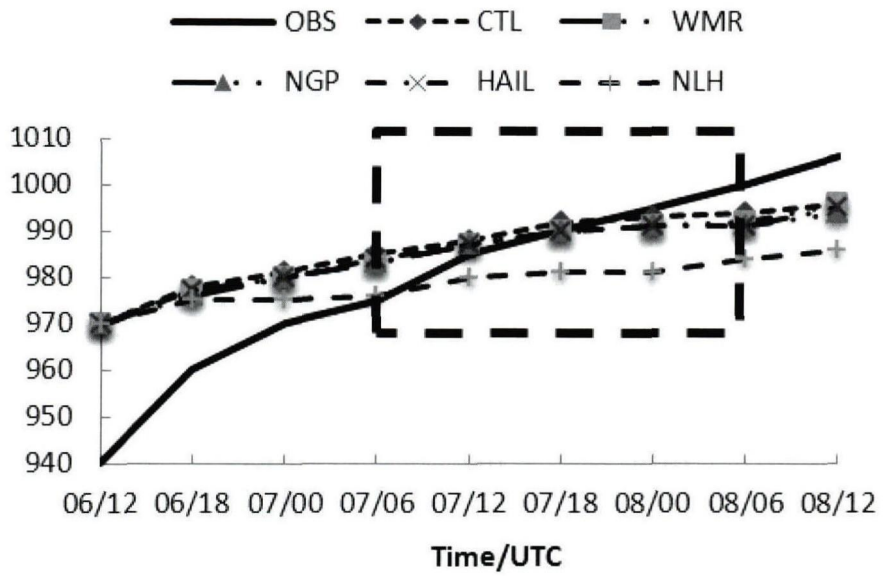

Figure 1. Comparison of the time series of minimum sea level pressure (units: hPa) from observation and all five simulations during the period of 1200 UTC 6 October to 1200 UTC 8 October.

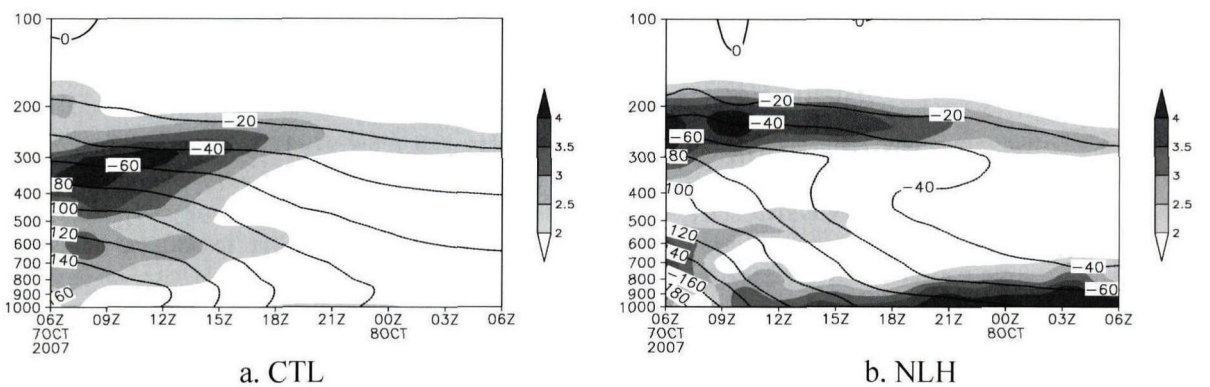

Figure 2. Temperature (shaded, units: ℃) and height (units: dagpm) anomalies at storm center during the period of 0600 UTC 7 October to 0600 UTC 8 October.

temperature and height anomalies (Fig.2), after 1500 UTC 7 October, warm core can be figured out below 800 hPa in NLH due to the absence of evaporation by cloud base and precipitation. Negative height field anomaly below 900 hPa is slightly larger in NLH than that in CTL as well. Thus, the low-level warm core is the main cause of lower sea level pressure. In the meantime, height field anomaly at mid-upper level in NLH is much smaller than that in CTL, which denotes that the storm will experience a rapid decrease in intensity without condensation (sublimation) latent heat. Overall, after the landfall of TCs, latent heat release contributes to the maintenance of intensity and structure.

Figure 3 compares the tracks of sensitivity experiments with observation. In general, there's little difference between each sensitivity experiment before Krosa's landing with a little north deviation than observation. After landing mainland, as the intensity variation (Fig.1) and precipitation distribution (Fig.4d, 4e) of NGP and HAIL are similar to CTL, the simulated tracks of NGP and HAIL are also relatively close to CTL. Simulated storms from these three experiments are all combined with mid-latitude westerly trough and move northeastward after landing. In experiment WMR, typhoon cloud structure becomes loose after landing, and therefore cold air from north involves into the core area (figure omitted). As a result, the storm moves southeastward. Simulated typhoon in NLH still maintains the integrity of low-level circulation after landing, and is not significantly affected by westerly trough. It continues to move northwestward along the west side of subtropical high. From the analysis above, it seems that microphysical processes have a certain influence on typhoon tracks after landing, in which ice-phase microphysical process and latent heat release show greater impact on track simulation.

3.2 *Horizontal distribution of 6-h accumulated rainfall*

Hua and Liu has compared the simulated 6-h accumulated rainfall in CTL with the observed one carefully[9]. As shown in Fig.4a, the observation showed

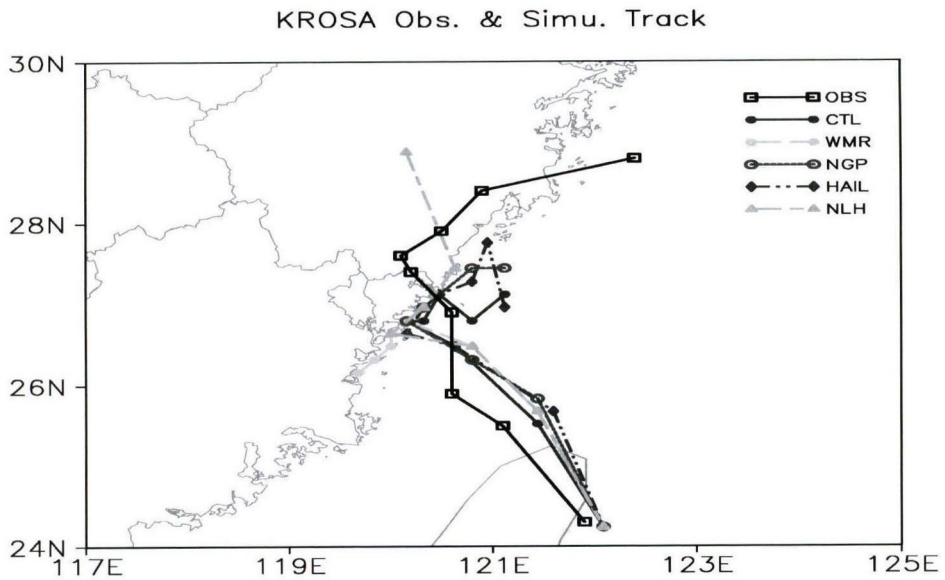

Figure 3. Comparison of the 6-hourly STI-CMA best track and the simulated tracks of Typhoon Krosa during the period of 1200 UTC 6 October to 1200 UTC 8 October.

asymmetry with stronger intensity in north and east sides of the rainbands with a maximum value of 24-h accumulated rainfall exceeding 100mm. The model could simulate the general features of rainfall distribution and intensity (Fig.4b). To the end of the simulation, spiral rainbands and the eye of typhoon shown by surface precipitation are still obvious, indicating that the storm can maintain its structure for a while after landing. In the late simulation, simulated storm is a bit more southward from the observation, thus the convergence in the south tends to be stronger, resulting in heavier local rainfall.

As shown in Fig.4c, rainfall distribution in experiment WMR is similar to that in CTL, but with a relatively uniform intensity. The maximum 6-h accumulated rainfall in WMR does not exceed 80 mm, and no obvious rainfall center is seen. In the meantime, precipitation in east and north sides of typhoon maintains in a range of 30 to 60 mm. After 0000 UTC 8 October, the typhoon structure becomes loose with weakening intensity. Cold air from north and moist warm air from the sea meet at central and southern Jiangsu province, and outer rainbands become precipitation center. Thus, without allowing the presence of ice particles leads to relatively uniform rainfall intensity. In other words, ice-phase process plays an important role in the maintenance of rainfall intensity and spiral rainbands, especially in the formation of heavy local rainfall.

As can be seen from Fig. 4d, the intensity and distribution of 6-h accumulated rainfall in NGP are between CTL and WMR. From 1800 UTC 7 October to 0600 UTC 8 October, NGP shows a similar precipitation center with CTL but with a weaker intensity (80 mm). The evolutions of rain belt in NGP and WMR seem alike, which means that the eye and spiral rainbands both become vague since 0000 UTC 8 October. The precipitation feature in NGP proves that adding ice and snow particles on the base of WMR can help increasing precipitation intensity. However, formation of local heavy rainfall and persistence of outer rainbands still call for bigger ice particles like graupel.

There is no significant change in surface precipitation in HAIL compared with CTL (see Fig.4e). From 1800 UTC 7 October to 0000 UTC 8 October, the maximum value of heavy rainfall at south Jiangsu province is 90 mm, slightly weaker than in CTL. Thus, hail has little impact on surface precipitation during this typhoon process.

In experiment NLH (Fig.4f), the horizontal structure of typhoon is difficult to distinguish through surface precipitation. The typhoon eye is fully filled and surface precipitation increases a lot. Areas with more than 100 mm rainfall are mainly found at southeast part and coastal area of Zhejiang province. Heavy rainfall regions begin to shrink since 1800 UTC 7 October, but the overall precipitation intensity does not change significantly. This result indicates the importance of latent heat release to the persistence of wide range precipitation.

3.3 *Vertical distribution of cloud microphysics*

The 6-h accumulated precipitation reaches a maximum at 0000 UTC 8 October. Therefore a cross section (see Fig.4) across precipitation center is made at this time to analyze the vertical structure of microphysics. Downdrafts dominate the eye of typhoon. Seen from Fig. 5a, cloud water mainly distributes at mid-level atmosphere between 400 to 700 hPa, with a maximum value of 0.09 g/kg appearing in the vicinity

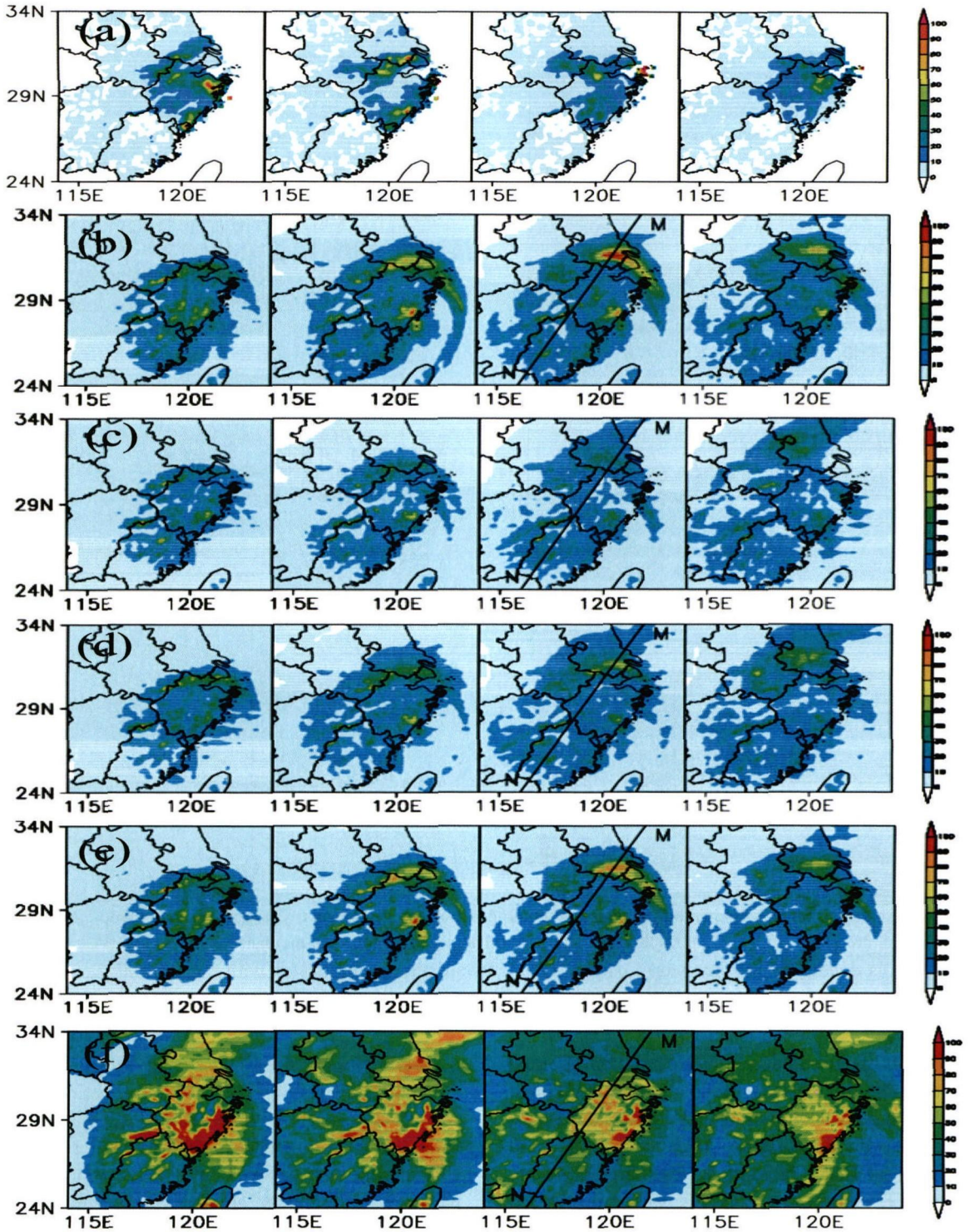

Figure 4. Horizontal distribution of the 6-h accumulated rainfall (units: mm) from the observations and 3.3-km grid simulations from 0600 UTC 7 October to 0600 UTC 8 October. a. OBS; b. CTL; c. WMR; d. NGP; e. HAIL; f. NLH.

of 0℃ isotherm. A small amount of cloud water exists in the form of supercooled water above melting layer. In the lower level, there's little cloud in the eye, while in the eyewall cloud base reaches as low as the ground. Rainwater (see Fig.5b) is concentrated in the mid-lower level below 0℃ layer with the maximum value appearing around 650 hPa. Precipitation center located at 120°E, 32°N corresponds to the high value area of rain water with a maximum of 1.0 g/kg. Since the drag effect of precipitation, obvious downdrafts are observed near surface layer. Cloud ice (Fig.5c) and snow (Fig.5d) are mostly located in the updrafts between 100 to 450 hPa with peak concentration of 0.08 g/kg and 0.27 g/kg respectively. Graupel forms through collision of ice particles and grows very quickly by both vapor deposition and collecting liquid and solid particles as it

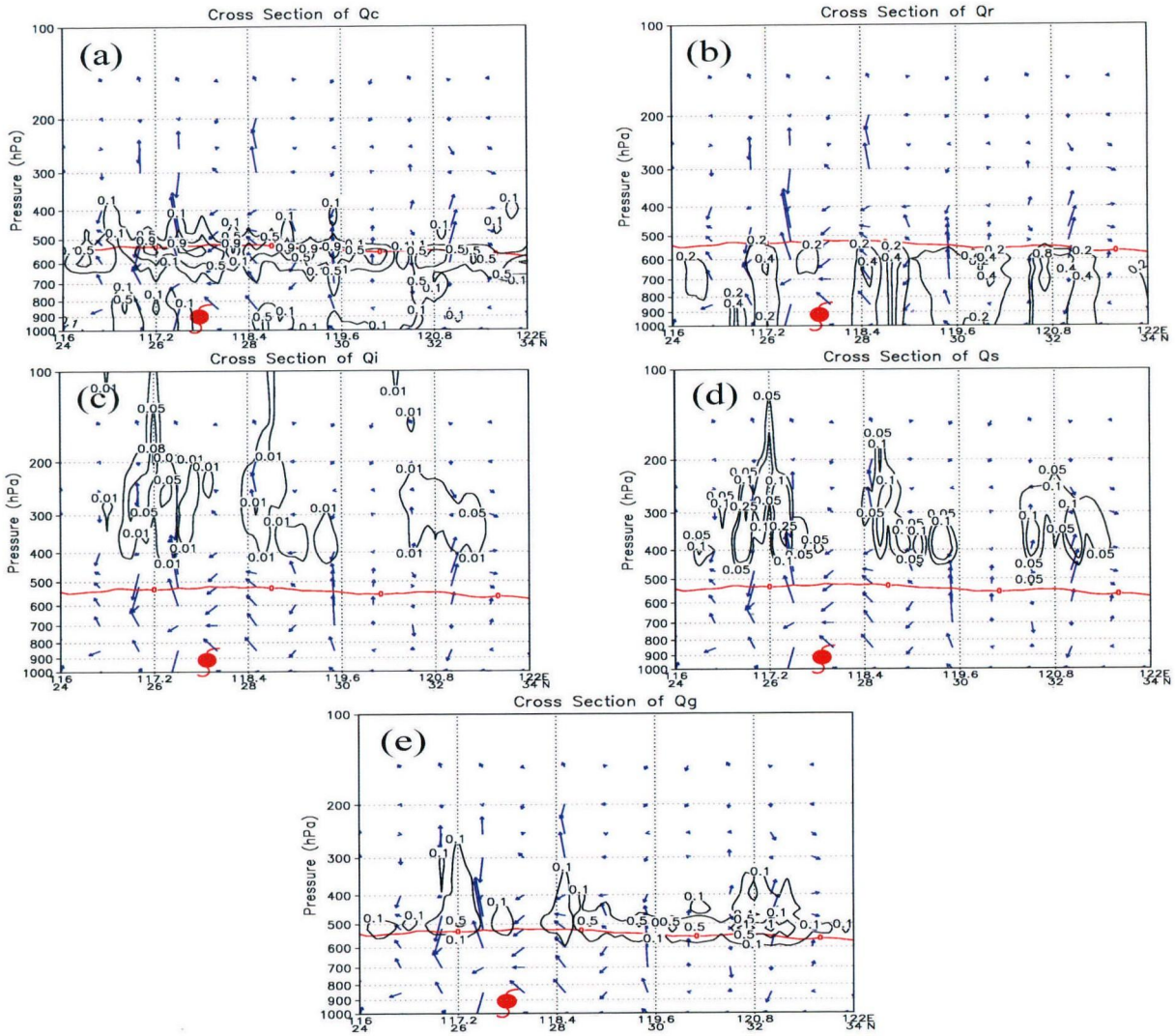

Figure 5. Cross sections along MN of the mixing ratios (units: g/kg) of (a) cloud water, (b) rainwater, (c) cloud ice, (d) snow and (e) graupel which are taken from CTL at 0600 UTC 8 October. The solid lines denote the distribution of the 0℃ isotherm. The typhoon symbols denote the surface storm center. The arrows denote wind vector with the vertical motion magnified 100 times.

falls (Fig.5e). A high value layer of graupel is observed around 500 hPa with a maximum of 1.30 g/kg. Graupel melts into rain as it falls through the melting level with a rapid reduction in concentration.

As can be seen from Fig.6, due to the weaker cooling effect caused by phase change in WMR, updrafts in the eyewall are enhanced in mid-level troposphere. The distribution of cloud water is significantly enlarged and extends to the top layer in the absence of ice particles. Taking into account there is thresholds in the microphysics scheme for rainwater evaporation and condensation and auto conversion from cloud water to rainwater (such as rainwater fall velocity must be greater than 10-4 m/s, and environment temperature must be greater than 243.15K), thus there' s no rainwater forms above 300 hPa (Fig.6b). Compared with CTL, there is less rainwater in WMR due to the absence of conversion from ice particles to rain, which is particularly evident in the vicinity of eyewall.

The contents of cloud ice (Fig.7c) and snow (Fig. 7d) are significantly increased in NGP, and the peak value layer of graupel declines to 300-400 hPa. Considering the fall velocity of cloud ice and snow particles is less than graupel, the existence of these small ice particles need not rely on strong updrafts, and is also easier to spread to a wider range. The concentration of cloud ice and snow particles in mid-level atmosphere weakens the updrafts around 500 hPa, which is more obvious in the north side of the storm. Weakened upward move ment further impacts water vapor convergence, which to some extent explains the decrease in surface precipita tion. Compared with CTL, removing graupel takes an increasing in cloud water content (Fig.7a). Moreover, due to the lack of efficient collisions of large ice particles, rainwater formation is hindered and surface precip itation is de

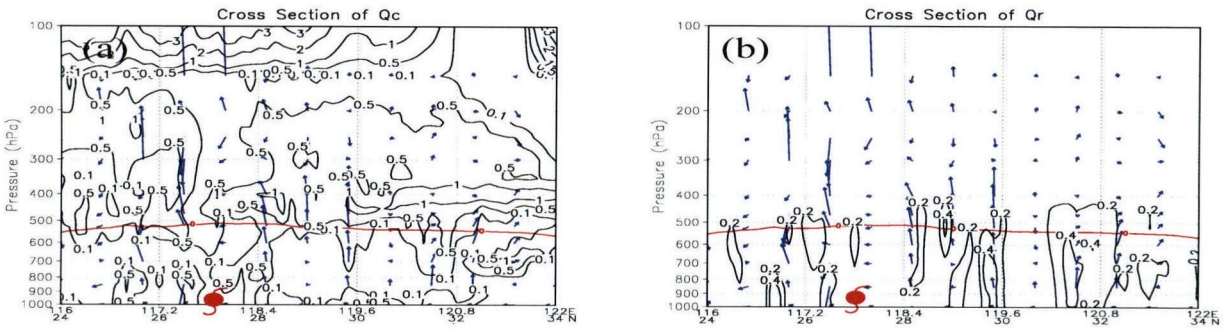

Figure 6. Cross sections along MN of the mixing ratios (units: g/kg) of (a) cloud water, (b) rainwater which are taken from WMR at 0600 UTC 8 October. Other instructions are as in Fig.5.

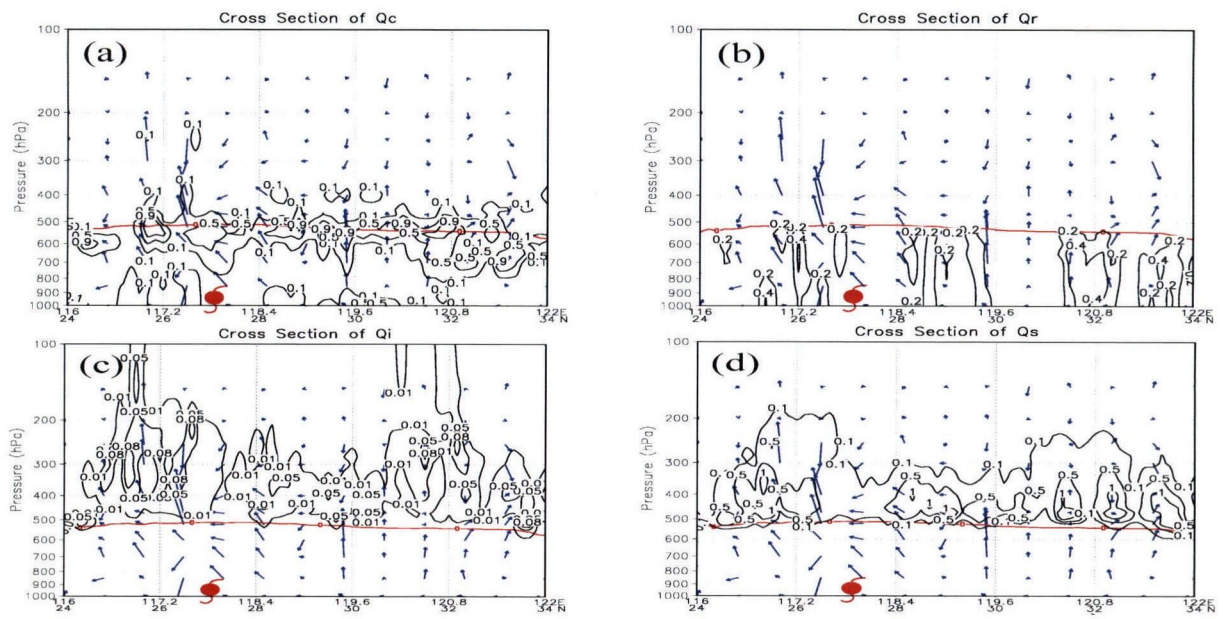

Figure 7. Cross sections along MN of the mixing ratios (units: g/kg) of (a) cloud water, (b) rainwater, (c) cloud ice and (d) snow which are taken from NGP at 0600 UTC 8 October. Other instructions are as in Fig.5.

creased (Fig.7b).

Figure 8 shows the results of experiment HAIL. Hail (Fig.8f) concentrates mainly between 400 to 500 hPa, and its distribution and peak area are similar to graupel (Fig.8e), which indicates the importance of graupel particles in the formation of hail. Li et al. has pointed out that conversion of graupel and hail is the main source of hail[16]. Since the convection in typhoon cloud systems is relatively weak after landing, it is difficult to generate large amount of hail particles. As a result, hail content is an order of magnitude smaller than graupel content. Therefore, graupel shows no significant change compared to control experiment. With a larger terminal velocity, in the 119-122°E region where hail has a higher concentration, drag effect makes updrafts weaker than in CTL. In this case, subject to environmental conditions, hail formation process is not significant, and therefore the addition of hail has little impact on other particles.

As can be seen from above analysis (Fig.4f), surface rainfall increased a lot in NLH with the removal of latent heat release. Fig.9 further shows that on the one hand, upper-level warm core is enhanced due to evaporation deduction (Fig.9b). Influenced by that, upper-level updrafts are also enhanced and cold cloud fully develops. Cloud ice (Fig.9c) and snow (Fig.9d) contents increase remarkably and spread to a wider range. Maximum of ice and snow reaches 0.08 g/kg and 0.35 g/kg respectively. Under favorable dynamic conditions, graupel (Fig.9e) extends to 200 hPa with a peak value of 2.0 g/kg. Plenty ice particles favor the formation of cloud water and rainwater (Fig.9a and 9b). Cloud water shows a bimodal vertical distribution (Fig. 9a). Part of cloud water is lifted above melting level and presents in the form of supercooled water. On the other hand, downdrafts at mid-lower level are enhanced obviously as a result of drag effect by precipitation. Thus, typhoon without latent heat release has a stronger vertical motion, which affects the content and distribution of hydrometers. In other words, feedback from thermal field to dynamic field is an important factor affecting the structure of clouds and precipitation

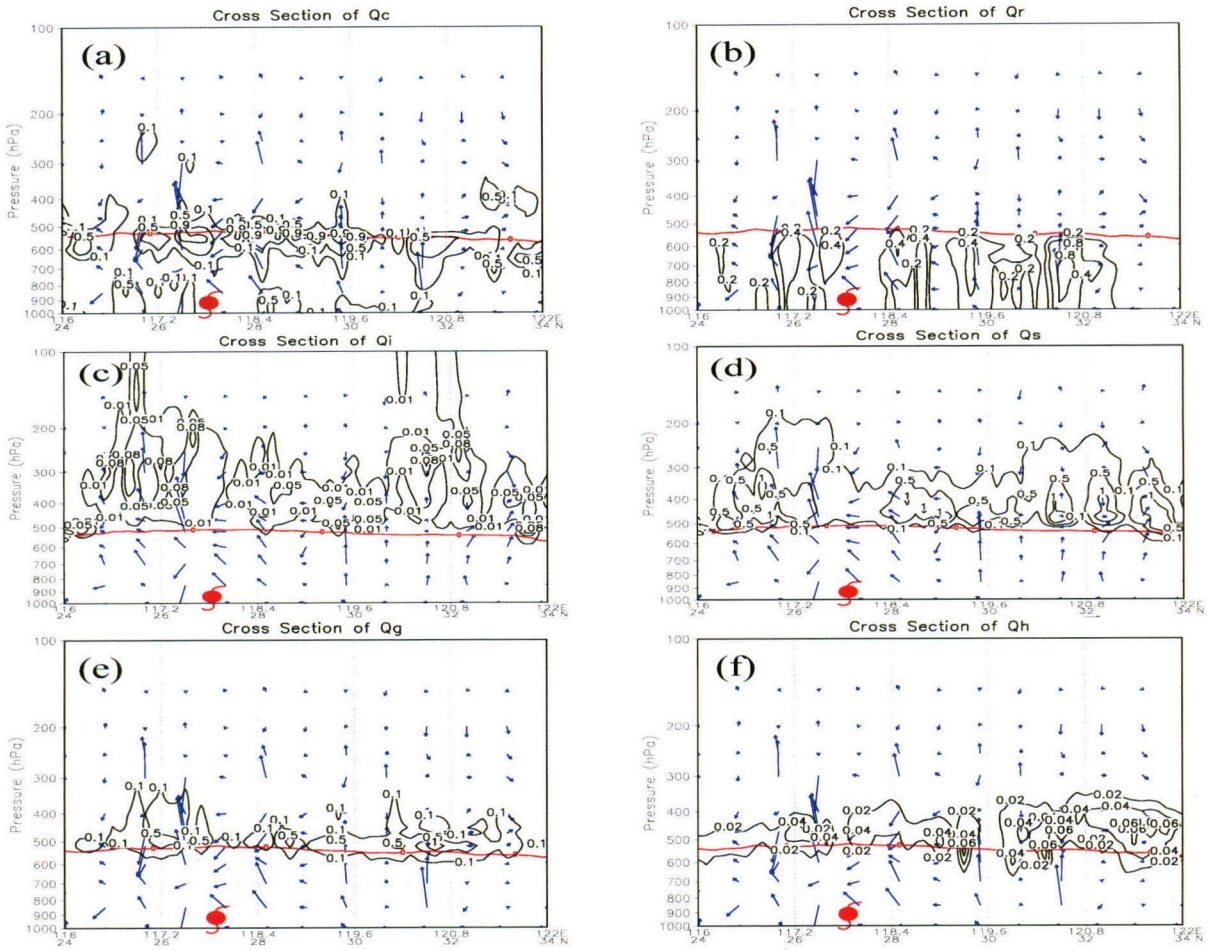

Figure 8. Cross sections along MN of the mixing ratios (units: g/kg) of (a) cloud water, (b) rainwater, (c) cloud ice, (d) snow and (e) hail which are taken from HAIL at 0600 UTC 8 October. Other instructions are as in Fig. 5.

in real typhoon.

3.4 *Typhoon vertical structure*

Vertical distributions of simulated radar reflectivity, wind vector and temperature anomalies are analyzed in this section to learn more about the sensitivity of different experimental designs. Hua and Liu has compared the horizontal reflectivity structure of control experiment and observation in detail, therefore here focus on the vertical structure [9]. Choose 0000 UTC 8 October, when precipitation becomes heavy and steady, to analyze the vertical structure. Observation from Jinhua station which is located near the typhoon eye is used as reference (location of Jinhua station and cross section are shown in Fig. 4a, and with the elevation angle of 0.5 degree). As shown in Fig. 10, reflectivity of more than 10 dBZ extends to 9 km height (corresponding to about 300 hPa), while stronger echo with reflectivity of more than 30 dBZ appears in mid-lower layer below 6 km (corresponding to about 500 hPa).

Reflectivity structure and strong echo position of CTL and observation are relatively alike, which indicates the realness of control experiment. Warm core formed by latent heat release occurs between 250 to 450 hPa, and radar reflectivity mainly appears in warm region below 500 hPa. Above 500 hPa the echo intensity decreases sharply. However, in the eyewall where strong convection exists, top of reflectivity reaches up to 200 hPa. Reflectivity is weak in the eye where downdrafts dominate, indicating no significant precipitation particle generates. Strong reflectivity is seen between 31-32° N with a central intensity of 40 dBZ. Compared with the vertical distribution of microphysics (Fig.5), it can be seen that content of hydrometer particles is relatively high in this region. Simulation results above are consistent with previous observations and simulations (Zhang[4]; Rogers et al.[17]).

In mid-upper troposphere, condensation from water vapor to cloud water enlarges warm core region in WMR, and warm area with temperature higher than 2℃ extends up to 200 hPa (Fig.11b). Radius of typhoon eye is larger and eye area is clear sky. Similar with control experiment, reflectivity in WMR mainly concentrates in warm region below 500 hPa, and the intensity and distribution are relatively uniform. The maximum reflectivity is only 30 dBZ due to weak precipitation.

Reflectivity structure in NGP is very different from that in CTL (Fig.11c). Instead of graupel, cloud ice and

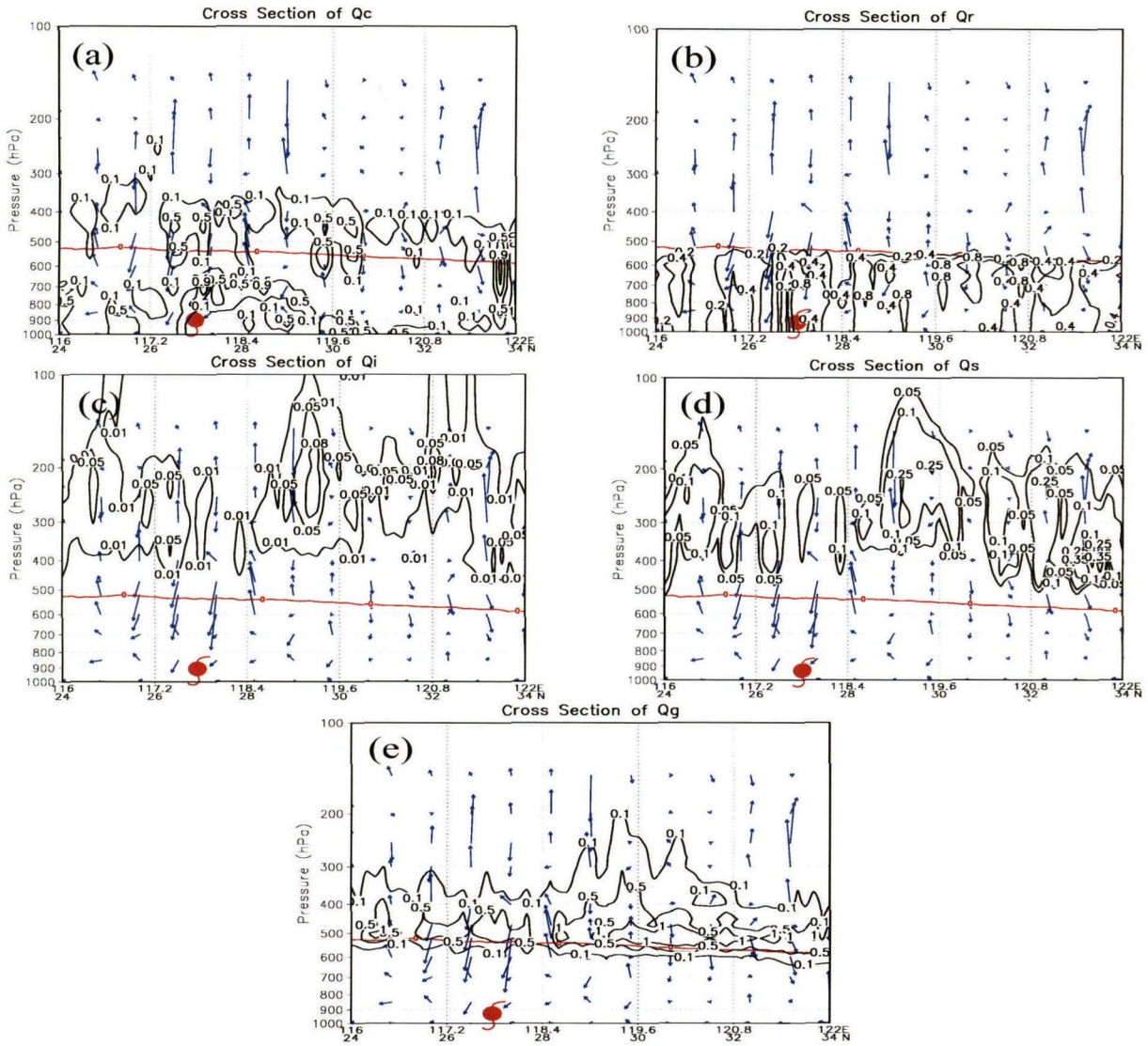

Figure 9. As in Fig. 5 but from NLH.

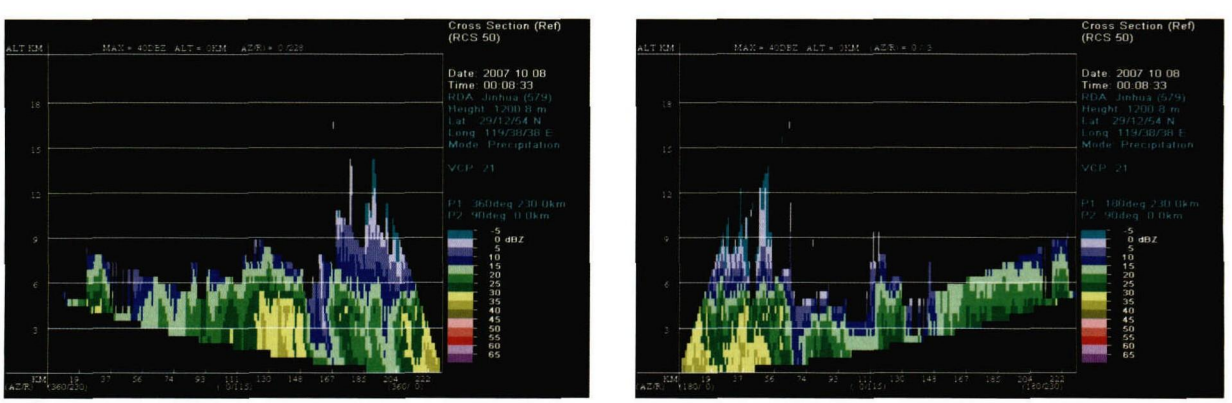

Figure 10. Cross sections of radar reflectivity (units: dBZ) through storm center in Jinhua station at 0000 UTC 8 October. The positions of radar station and cross section are shown with red angle and line LL1 respectively in Fig.4a.

snow particles concentrate above melting level, so that the reflectivity mainly distribute between 300 to 500 hPa. Lower content of rainwater leads to sharp reduction in reflectivity intensity below 500 hPa. Updrafts around typhoon eye are weak, and warm region with temperature higher than 2 ℃ is small. Besides, it is very hard to distinguish the eye from radar echoes. In summary, typhoon structure and precipitation are very sensitive to graupel. Simulation results will deviate significantly from real situation in absence of

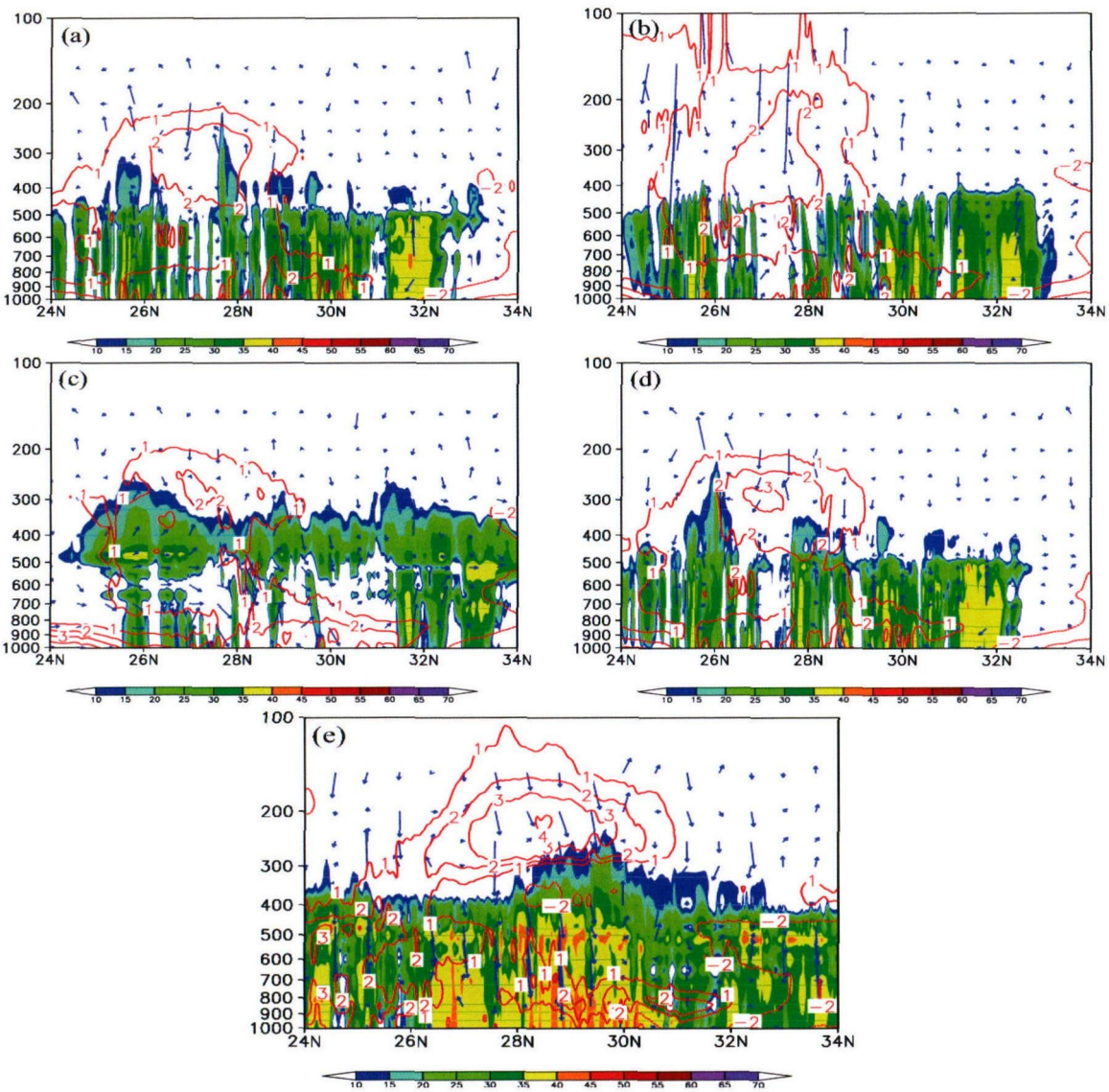

Figure 11. The north-south cross sections of temperature deviations, at intervals of 1 ℃, and in-plane flow vectors and radar reflectivity (units: dBZ) through the eye center in Jinhua station at 0000 UTC 8 October for (a) CTL (red box for Jinhua radar detection range), (b) WMR, (c) NGP, (d) HAIL and (e) NLH.

graupel particles.

Adding hail into microphysical scheme leads to a stronger storm (Fig.11d). A closed 3℃ temperature anomaly contour is observed near typhoon center in HAIL. Convective clouds in eyewall extend up to 200 hPa. Rainband distribution and reflectivity intensity are similar with that in CTL. Seen from above analysis, in this case, addition of hail can help enhancing warm core structure to some extent. However, it has little effect on overall structure of typhoon.

Similar with results in Fig.2b, Fig. 11e shows that there are two warm cores in NLH locate between 200 to 300 hPa and below 900 hPa respectively. The main cause of these two warm cores is reduction of evaporation at cloud top and cloud base. Due to abundant hydrometer particles, reflectivity intensity enhances significantly, and the echo top raises up to 400 hPa. Moreover, the typhoon eye is fulfilled.

4 CONCLUSIONS

(1) Typhoon tracks can be influenced by changes in microphysics process and latent heat release, resulting in simulation results very different from observation. However, typhoon intensity is not sensitive to varying microphysics. Landing typhoon without latent heat release shows warm low pressure near surface layer, and intensity in mid-upper troposphere decreases rapidly.

(2) Ice-phase processes play an important role in the formation of local heavy precipitation and persistence of spiral rainbands. Removal of ice-phase processes leads to relatively uniform distribution and weaker intensity in precipitation. In WMR, cloud water spreads to a wider range and has a higher content. Due

to the lack of conversion from ice particles to rainwater, both rainwater content and surface precipitation have decreased.

(3) Microphysical processes associated with graupel particles play an important role in typhoon simula tion. Results from experiment NGP show that, both surface precipitation and spiral rainbands decrease without graupel particles. Increase in ice and snow content indicates that collisions among graupel, cloud ice and snow particles are one of main sink of cloud ice and snow. The main range of radar reflectivity raises up to middle troposphere between 300 to 500 hPa with removal of graupel, and typhoon eye is fully filled.

(4) Since the convection is not strong enough, hail growth meets restriction. And hail particles have little impact on surface precipitation and cloud structure in this case.

(5) Hydrometer contents and surface precipitation increase significantly and typhoon eye is fulfilled without latent heat release. Latent heat process influences content and distribution of hydrometers through feedback on dynamic field.

REFERENCES:

[1] DONG Mei-ying, CHEN Lian-shou, ZHENG Pei-jun, et al. Research progress of abrupt intensification of heavy rainfall and super heavy rainfall associated with landfalling tropical cyclones [J]. J Trop Meteorol, 2009, 25 (4): 495-502.

[2] LI Jiang-nan, WANG An-yu, YANG Zhao-li, et al. Advancement in the study of typhoon rainstorm[J]. J Trop Meteorol, 2003, 19 (suppl.): 152-159.

[3] CHEN Lian-shou, LUO Zhe-xian, LI Ying. Research advances on tropical cyclone landfall process [J]. Acta Meteor. Sinica, 2004, 62(5): 541-549.

[4] ZHANG Da-lin. Roles of various diabatic physical processes in mesoscale models [J]. Chinese J. Atmos. Sci., 1998, 22(4): 548-561.

[5] WANG, Y. An explicit simulation of tropical cyclones with a triply nested movable mesh primitive equation model: TCM3 Part II: Model refinements and sensitivity to cloud microphysics parameterization [J]. Mon Wea Rev, 2002, 130(12): 3022-3036.

[6] ZHU T, ZHANG D L. Numerical Simulation of Hurricane Bonnie (1998) Part II: Sensitivity to varying cloud microphysical processes [J]. J Atmos Sci, 2006, 63 (1): 109-126.

[7] FRANKLIN C N, HOLLAND G J, MAY P T. Sensitivity of tropical cyclone rainbands to ice-phase microphysics[J]. Mon Wea Rev, 2005, 133(8): 2 473-2 493.

[8] CHENG Rui, YU Ru-cong, FU Yun-fei, et al. Numerical research on intensity change and structure feature of Typhoon Rananim near shore. I: Impact of cloud microphysical parameterization on cloud structure and precipitation features [J]. Acta Meteorol Sinica, 2009, 67 (5): 764-776.

[9] HUA Cong, LIU Qi-jun. Numerical simulation of cloud microphysical features of landfall typhoon Krosa[J]. J Trop Meteorol, 2011, 27(5): 626-638.

[10] CHEN Xiao-min. Numerical simulation study on microphysical structure and cloud seeding in summer cloud system of the Qilian mountain region [D]. Beijing: Chinese Academy of Meteorological Sciences, 2007.

[11] WANG Si-min, YIN Yan. A numerical simulation of cloud microphysical processes of a tropical convective cloud [J]. J Trop Meteorol, 2011, 27(4): 519-528.

[12] MCCUMBER M, TAO W K, SIMPSON J. Comparison of ice-phase microphysical parameterization schemes using numerical simulation of tropical convection [J]. J Appl Meteorol, 1991, 30(7): 985-1004.

[13] HU Zhi-jin, HE Guan-fang. Numerical simulation of microprocesses in cumulonimbus clouds (I) microphysical model [J]. Acta Meteorol Sinica, 1987, 45(4): 467-484.

[14] YU Da-wei, He Guan-fang, Zhou Yong, et al. Three-dimensional convective cloud seeding model and its field application [J]. Quart J Appl Meteorol, 2001, 12 (suppl): 122-132.

[15] DING Yi-hui. Advanced Synoptic Meteorolo gy [M]. Beijing: China Meteorological Press, 2005: 289-290.

[16] LI Shu-ri, HU Zhi-jin, WANG Guang-he. Improvement and simulation of three-dimension convective cloud seeding model of CAMS[J]. Quart J Appl Meteorol, 2003, 14 (suppl): 78-91.

[17] ROGERS R F, BLACK M L, CHEN S S, et al. An evaluation of microphysics fields from mesoscale model simulations of tropical cyclones Part I: Comparisons with observations [J]. J Atmos Sci, 2007, 64(6): 1 811-1 834.

Citation: HUA Cong and LIU Qi-jun. Sensitivity of landfalling typhoon structure and precipitation to varying cloud microphysical processes [J]. J Trop Meteorol, 2016, 22(3): 341-351.